ORIGINAL ARTICLE

Actively priming autophagic cell death with novel transferrin receptor-targeted nanomedicine for synergistic chemotherapy against breast cancer

Dong Mei[a,b], Binlong Chen[b], Bing He[b], Haibin Liu[c], Zhiqiang Lin[d], Jialiang Lin[b], Xiaoyan Zhang[a], Ning Sun[a], Libo Zhao[a], Xiaoling Wang[a,*], Qiang Zhang[b,*]

[a]Clinical Research Center, Beijing Children's Hospital, Capital Medical University, National Center for Children's Health, Beijing 100045, China
[b]Key Laboratory of Molecular Pharmaceutics, New Drug Delivery Systems, School of Pharmaceutical Sciences, Peking University, Beijing 100191, China
[c]Department of General Surgery, China-Japan Friendship Hospital, Beijing 100029, China
[d]Institute of Systems Biomedicine, School of Basic Medical Sciences, Peking University Health Science Center, Beijing 100191, China

Abstract   Recently, considerable attention in the field of cancer therapy has been focused on the mammalian rapamycin target (mTOR), inhibition of which could result in autophagic cell death (ACD). Though novel combination chemotherapy of autophagy inducers with chemotherapeutic agents is extensively investigated, nanomedicine-based combination therapy for ACD remains in infancy. In attempt to actively trigger ACD for synergistic chemotherapy, here we incorporated autophagy inducer rapamycin (RAP) into 7pep-modified PEG-DSPE polymer micelles (7pep-M-RAP) to specifically target and efficiently priming ACD of MCF-7 human breast cancer cells with high expression of transferrin receptor (TfR). Cytotoxic paclitaxel (PTX)-loaded micelle (7pep-M-PTX) was regarded as chemotherapeutic drug model. We discovered that with superior intracellular uptake *in vitro* and more tumor accumulation of micelles *in vivo*, 7pep-M-RAP exhibited excellent autophagy induction and synergistic antitumor efficacy with 7pep-M-PTX. Mechanism study further revealed that 7pep-M-RAP and 7pep-M-PTX used in combination provided enhanced efficacy through induction of both apoptosis- and

mitochondria-associated autophagic cell death. Together, our findings suggested that the targeted excess autophagy may provide a rational strategy to improve therapeutic outcome of breast cancer, and simultaneous induction of ACD and apoptosis may be a promising anticancer modality.

1. Introduction

Cancer is the leading cause of death around the world, and chemotherapy is the most widely used treatment in clinic[1]. However, the efficacy of monotherapy is usually limited in clinic due to the complexity and refractory of cancer. Whether it is treated by conventional cytotoxic drugs or molecularly-targeted therapeutics, the drug resistance, insufficient curative effect and tumor relapse are still the huge challenges[2,3]. With the increased understanding of the mechanisms underlying the compromised therapeutic efficacy of monotherapy, combination therapy with two or more therapeutic agents generally acting on multiple therapeutic targets, or one increasing the sensitivity of tumor cells to another one, has increasingly become a standard practice in clinic[4,5]. In particular, as more and more regulators of signaling proteins or pathways which play key roles in oncogenic transformation and drug resistance are identified, the combined strategies of these regulators with the current chemotherapeutics are being studied extensively for cancer treatment[6,7].

Novel combinations of small molecularly targeted agents with chemotherapy, have gained increasing attention in research that aims to overcome drug resistance and tumor heterogeneity for highly effective cancer regimens. Rapamycin (RAP), a mammalian target of rapamycin (mTOR) inhibitors, was developed as a potential anticancer drug, including lung, cervix, colon and breast cell carcinomas[8]. Studies have found that RAP or its derivatives enhanced the antitumor efficacy of taxane chemotherapeutic agents (*e.g.*, paclitaxel (PTX)) in many clinical trials[9,10] by targeting the mTOR protein, which is centrally involved in angiogenesis, cell survival, proliferation and metabolism[11−14]. The currently reported synergistic anti-tumor mechanism of combined RAP or its derivatives with PTX mainly involves the anti-angiogenesis effect of RAP and its direct inhibition of mTOR in tumor development[15,16].

In addition, RAP is the most commonly used agent to induce autophagy. Recent evidence has indicated that tumor suppression following RAP treatment is linked to the induction of autophagic cell death (ACD)[17,18]. Autophagy is a highly regulated process that degrades or recycles bulk cytoplasmic constituents through lysosome-based pathway, resulting in the formation of a double-membranous structure, which is termed as an autophagosome in eukaryotic cells. The autophagic process is robustly upregulated in response to cellular stress, and it is known to be involved in a multitude of cellular processes including immunity, programmed cell death, the selective degradation of organelles, tumor, aging and numerous neurodegenerative conditions, while its precise role in the development of tumors is ambiguous[19,20]. Although some evidence suggested that autophagy promotes cell survival under nutrient deprivation, a growing body of evidence revealed that autophagy plays an inhibitory role in the process of tumor formation, suggesting that autophagy may be an excellent mechanism for tumor suppression[21]. Although the anti-tumor efficacy of RAP combined with PTX in breast cancer has been verified in preclinical and clinical trials, the relationship between autophagy and synergistic effect of this combined strategy is not well understood, despite the effectiveness of RAP in induction of ACD.

It's worth noting that the clinical outcome of current combination therapy based on conventional pharmaceutical preparations is unsatisfactory, due to the short half-lives of chemotherapeutic agents and lack of distribution selectivity, leading to severe side effects and deficient therapeutic efficacy[22]. Nanotechnology-based targeted delivery systems provide good opportunity to address the associated problems and provide superior therapeutic benefits[23]. Some antitumor nanomedicines, such as Doxil® (PEGylated liposomal doxorubicin) and Abraxane® (PTX (PTX) loaded albumin nanoparticles), have been approved by FDA for more than 10 years[24]. Nanomedicines can selectively deliver cargos to cancerous cells through passive targeting based on enhanced permeation and retention (EPR) effect, as well as active mechanisms based on molecular recognition between the overexpressed receptor/antigen on cancerous cells with the targeting molecules on the surface of nanocarriers[25]. Transferrin receptor (TfR) is overexpressed in various cancer cells, making it an excellent target for tumor recognition. 7pep (7pep, Histidine-Alanine-Isoleucine-Tyrosine-Proline-Arginine-Histidine, HAIYPRH) is a peptide obtained through phage display and has exhibited high affinity to TfR. Thus, 7pep can serve as an effective ligand for cancer-targeted drug delivery systems[26,27].

Therefore, based on the above background, we developed a 7pep-modified dual-nanomedicines system that loaded RAP and PTX separately to examine the efficacy and safety in the treatment of breast cancer, while focusing on the role of RAP-induced autophagy in the combined anti-tumor efficacy. It is expected that the dual-nanomedicines administered in combination can actively accumulate in tumor sites *via* TfR-mediated mechanism and achieve favorable anti-tumor effect compared to monotherapy. It is well known that the nanomedicine has a great influence on pharmacokinetics, such as drug release, absorption, and distribution behavior[28], but underlying anti-tumor mechanism of co-administration of nanomedicines has been rarely reported. In particular, autophagy is a dynamic process that correlates with cellular status, drug concentration, administration schedule and sequence, it is necessary to explore the role of autophagy in the synergic effect of dual-nanomedicines in combination. Firstly, a functional material with TfR targeting ability was synthesized through the conjugation of 7pep to PEG-DSPE copolymer, and then functional nanocarriers were constructed by a solvent evaporation method. The active targeting efficacy of nanocarrier, superior autophagy inducibility of 7pep-RAP-M, anti-proliferation and pro-apoptotic effects of functional nanocarriers used alone or in combination in a human breast cancer cell line (MCF-7) were evaluated, followed by the *in vivo* distribution, antitumor efficacy and toxicity studies. Especially, the probable mechanisms

involved with this strategy of dual-nanomedicines were well explored.

2. Materials and methods

The materials, methods for cell culture, synthesis of functional copolymer 7pep-PEG-DSPE, preparation and characterization of the functional nanocarriers, as well as the determination of transferrin receptor expression on MCF-7 cells are shown in the Supporting Information Section 1. Materials and methods.

2.1. Cellular uptake study of single formulations

The cellular uptake of C6-loaded micelles was investigated by both flow cytometry and confocal microscopy. For the flow cytometry method, MCF-7 cells were seeded in 12-well plates and incubated for 24 h at 37 °C. Then cells were treated with various C6 formulations at a final C6 concentration of 100 ng/mL for 2 h at 37 °C. For receptor competitive experiments, cells were pre-incubated with excessive anti-CD71 antibody to saturate transferrin, followed by addition of C6 formulations. Then cells were trypsinized, washed with cold PBS, and re-suspended in PBS. Finally, the C6 fluorescence intensity was measured by a flow cytometer with 10,000 events collected. For confocal microscopy study, MCF-7 cells were cultured on coverslips for 24 h at 37 °C prior to experiment. Then cells were treated with various C6 formulations at a final C6 concentration of 100 ng/mL for 2 h. After washing with PBS for three times, cells were fixed with 4% paraformaldehyde for 15 min, followed by cell nuclei staining with Hoechst 33258 for 20 min at 37 °C. The sample was observed by a Leica TCS SP5 confocal laser scanning microscope (CLSM, Heidelberg, Germany).

2.2. The cellular uptake study of co-administration

MCF-7 cells were cultured on 12-well plates and incubated for 24 h. Then cells were treated with following various formulations for 2 h at 37 °C, including M-PTX, 7pep-M-PTX, M-PTX plus M-RAP added simultaneously, 7pep-M-PTX plus 7pep-M-RAP added simultaneously, M-PTX with M-RAP pretreatment for 6 h, 7pep-M-PTX with 7pep-M-RAP pretreatment for 6 h, respectively. The modification density of 7pep was 15%. The final concentrations of PTX and RAP in micellar solution were both 10 μmol/L. At the end of treatment, the amount of PTX or RAP in cells treated with different formulations was quantified by a HPLC system. The protein content of cells was determined by a BCA Protein Quantitation Kit according to the user manual.

2.3. Intracellular distribution of C6-loaded micelles

MCF-7 cells were cultured on coverslips for 24 h at 37 °C prior to experiment. After incubated with various C6 formulations at a final C6 concentration of 100 ng/mL for 2 h, cells were treated with pre-warmed (37 °C) LysoTracker Red-containing medium. Then, cells were fixed with 4% paraformaldehyde for 15 min and nuclear was stained with Hoechst 33258. Samples were imaged and analyzed by CLSM. Quantitative analysis of the colocalization efficiency was performed using Pearson's correlation coefficient by Image J (NIH, USA).

2.4. In vitro cytotoxicity assay

Sulforhodamine B (SRB) colorimetric assay[29] was applied to investigate the in vitro cytotoxicity of various drugs in single and combination use against MCF-7 cells. Concretely, MCF-7 cells were seeded in 96-well plates for 24 h at 37 °C. The cells were then treated with serial concentrations of free RAP, M-RAP, 7pep-M-RAP, free PTX, M-PTX, 7pep-M-PTX, free RAP plus free PTX (referred to as Free Combi group), M-RAP plus M-PTX (referred to as M-Combi group), 7pep-M-RAP plus 7pep-M-PTX (referred to as 7pep-M-Combi group) for 48 h. For combination therapy, RAP formulations were added 12 h before the treatment of PTX formulations. After incubation, the cells were fixed with 10% cold TCA for 1 h, followed by washing and drying. The fixed cells were then stained with 0.4% SRB for 30 min, washed by 1% acetic acid and dried. The bound dye was dissolved in 10 mmol/L Tris base solution and the absorbance was measured at 540 nm by a 96-well plate reader. The IC_{50} values (the drug concentration inhibiting cells growth by 50%) were calculated by SPSS software. The CI_{50} values (the combination index at 50% inhibition rate) was calculated by the following Eq. (1):

$$CI50 = \frac{(IC_{50}^{PTX})_{Combi}}{(IC_{50}^{PTX})_{Single}} + \frac{(IC_{50}^{RAP})_{Combi}}{(IC_{50}^{RAP})_{Single}} \tag{1}$$

The index of CI_{50} was used to assess the synergetic, additive or antagonistic effect of various PTX used in combination with RAP formulations[30].

2.5. Cell apoptosis analysis by flow cytometry

Cell apoptosis was evaluated by Annexin V-FITC/PI apoptosis detection kit. Briefly, MCF-7 cells were cultured in 6-well plates for 24 h, and treated with culture medium (negative control), free RAP, M-RAP, 7pep-M-RAP, free PTX, M-PTX, 7pep-M-PTX, Free Combi, M-Combi, 7pep-M-Combi for 24 h. For combination therapy, RAP formulations were added 12 h before the treatment of PTX formulations. The final concentrations of RAP and PTX were 100 and 10 nmol/L, respectively. At the end of treatment, cells were trypsinized, washed with cold PBS. Then cells were stained with Annexin V-FITC, followed by propidium iodide (PI). Finally, the cell apoptosis was analyzed by a flow cytometer with 10,000 events collected.

2.6. The mechanism study on the synergetic effect of combination therapy

2.6.1. The effect of autophagy inhibitor 3-MA on cytotoxicity and apoptosis

MCF-7 cells were cultured for 24 h at 37 °C. Then cells were treated with or without 3-MA for 6 h, followed by 7pep-M-RAP, 7pep-M-PTX, 7pep-M-Combi, respectively. For combination group, 7pep-M-PTX was added 12 h after 7pep-M-RAP. The final concentrations of RAP and PTX were 100 nmol/L and 10 nmol/L, respectively. After the addition of 7pep-M-PTX for 24 h, the cells were treated with SRB colorimetric assay, or analyzed by annexin V-FITC/PI apoptosis detection kit.

2.6.2. The inhibition effect of 3-MA on autophagic vesicular accumulation

The cellular autophagic vesicular accumulation in different treatment groups was determined by monodansylcadaverine

(MDC) staining, Cyto-ID® autophagy detection kit, transmission electron microscopy (TEM), the expression of the autophagy marker protein LC3B, as well as the LC3-II/LC3-I ratio detected by Western blot. MCF-7 cells were seeded on coverslips for 24 h and treated with different RAP or PTX formulation used in single or combination as described above.

2.6.2.1. MDC labeling. Drugs treated cells were stained with 10 μmol/L MDC at 37 °C for 15 min[31]. The cellular fluorescence was observed using fluorescence microscope (Olympus, FV1000, Tokyo, Japan).

2.6.2.2. Cyto-ID® autophagy detection dye staining. After treated with drugs for 24 h, cells were stained with Cyto-ID® autophagy detection dye plus Hoechst 33342 at 37 °C for 30 min. Stained cells were then photographed with a CLSM, or analyzed by flow cytometer. The excitation and emission wavelengths for Cyto-ID dye were 488 and 560 nm, respectively.

2.6.2.3. ELISA analysis and immunofluorescent staining of LC3B. Briefly, for ELISA analysis, after treated with drugs for 24 h, cells were lysed, centrifuged at $1500 \times g$ at 4 °C for 5 min. Samples containing LC3B were incubated in the wells of microplate pre-processed by antibody for 2 h. After being washed, the microplate was incubated with HRP-conjugate reagent for another 1 h. The substrates were added for color development in the dark for 30 min. The absorbance was measured at 450 nm and the expression ratio was calculated according to the user manual. For immunofluorescence staining, after treated with drugs, cells were fixed, incubated with anti-LC3B monoclonal antibody overnight at 4 °C, followed by staining with second antibody (Texas red labeled goat IgG). Negative control cells were incubated with 5% BSA solution instead of anti-LC3B antibody. Nuclei were labeled with Hoechst 33258 for 20 min at 37 °C. Finally, cells were observed using a CLSM.

2.6.2.4. Detection of LC3-II/LC3-I by western-blot. This experiment was carried out according to previous report[32]. Briefly, cell lysates were extracted by using sodium dodecyl sulfate-PAGE and transferred to a PVDF membrane. Then, it was incubated overnight with primary antibody against LC3B (rabbit, 1:1000) followed by HRP-conjugated goat anti-rabbit IgG (H + L). The target proteins were visualized by chemiluminescence after adding the developer (ChemiDoc XRS, Bio-Rad, Hercules, CA, USA). Protein expression was quantified by densitometric analysis with ImageJ software.

2.6.3. Effect of autophagy on the morphology and function of mitochondria
2.6.3.1. TEM. The drugs treated cells were harvested and fixed in 2.5% phosphate-buffered glutaraldehyde for 2 h. Thereafter, cells were washed with 0.1 mol/L phosphate buffer and fixed with 1% OsO_4 buffer for 20 min. Subsequently, cells were washed, dehydrated by an ascending ethanol gradient series, and finally embedded in pure acetone. Next, samples were solidified, cut to ultrathin sections, stained with 3% lead citrate plus uranyl acetate, and photographed using a TEM.

2.6.3.2. Colocalization of mitochondria with autophagic vesicles. At the end of dosing period, cells were washed with PBS, and stained with a mixture of Mitotracker deep Red and Cyto-ID® autophagy detection dye at 37 °C for 30 min. The fluorescent images were then captured by a CLSM. Mitochondrial autophagy was analyzed by colocalization of autophagic vesicles and mitochondria.

2.6.3.3. Mitochondrial membrane potential (MMP, ΔΨm). After exposed to various formulations with or without 3-MA for 24 h, the cells were harvested, washed with PBS, and stained with mitochondrial specific fluorescent probe JC-10 at 37 °C for 15 min. Fluorescence intensity of JC-10 accumulated in mitochondria was observed by a FAScan flow cytometer and CLSM.

2.6.3.4. Release of cytochrome c. The translocation of cytochrome C from mitochondria to the cytoplasm was examined by commercial ELISA kit. In brief, at the end of dosing period, cells were lysed, centrifuged at $3000 \times g$ at 4 °C for 20 min. Samples containing cytochrome c were incubated in the wells of microplate pre-processed by anti-cytochrome c antibody for 2 h. After being washed, the microplate was incubated with HRP-conjugate reagent for another 1 h. The substrates were added for color development in the dark for 15 min. The absorbance was measured at 450 nm and the relative release percent was calculated according to the user manual.

2.6.3.5. Intracellular ATP levels. The intracellular ATP levels in both control and drugs treated MCF-7 cells were measured by commercial ATP assay kit according to the manufacturer's instructions Concretely, the treated cells were lysed, and mixed with luciferase reagent in an opaque black 96-well plate. The ATP-dependent light emitted by the luciferase catalyzed oxidation of luciferin was then determined by a Fluoroskan Ascent FL (Thermo Scientific, MA, USA).

2.6.3.6. Caspase 9 and 3 activities. The activities of caspases 9 and 3 was determined using commercial luminescent assays kits. Briefly, after incubated with drugs, cells were lysed, centrifuged at $10,000 \times g$ at 4 °C for 1 min. Lysates were added into 96-well plates, and mixed with caspase 9 substrate or caspase 3 substrate, respectively. After mixture was incubated for another 4 h at 37 °C, the activity was measured at 405 nm on a microplate reader, and the activity ratio was calculated according to the user's instruction.

2.7. In vivo tissue distribution of nanocarriers by live imaging

The bio-distribution of 7pep-M-DiR in single use and in combination with 7pep-M-DiD was investigated in MCF-7 tumor-bearing female *nu/nu* nude mice using an *in vivo* imaging system. The MCF-7 mice model was established by orthotopical injection of 4×10^6 MCF-7 cells. For the study of targeted delivery of 7pep-modified nanocarriers in single use to tumor model, when tumor volume reached about 350 mm³, 200 μL of PBS, free DiR, M-DiR, 7pep-M-DiR, 7pep-M-DiR with blank 7pep-M pre-injection for 1 h, was intravenously injected *via* the tail vein at a dose of 100 μg/kg, respectively. For the study of the effect of co-administration on the bio-distribution of nanocarriers, mice were injected with 7pep-M-DiD, 7pep-M-DiR, 7pep-M-DiD plus 7pep-M-DiR, 7pep-M-DiD (pre-injected for 24 h) plus 7pep-M-DiR, respectively. At the predetermined time points, the mice were anaesthetized by isoflurane and imaged by an *in vivo* imaging system (Carestream Health, Fx Pro, USA). The fluorescent images were taken with an excitation at 748 nm and an emission at

780 nm for DiR, as well as an excitation at 630 nm and an emission at 700 nm for DiD. After imaging at the last time point, the mice were sacrificed, then tumors and major organs were excised to collect *ex vivo* fluorescent images.

2.8. In vivo therapeutic efficacy and toxicity studies

The MCF-7 tumor-bearing nude mice model described above was used to evaluate the therapeutic efficacy and toxicity *in vivo*. When the tumor volume reached $30-50$ mm^3, mice were injected with different RAP and PTX formulations in single or combination after randomization, including PBS (control), free RAP, M-RAP, 7pep-M-RAP, free PTX, M-PTX, 7pep-M-PTX, Free Combi, M-Combi and 7pep-M-Combi. Both free RAP and free PTX are prepared with Cremophor EL and ethanol (1:1, *v/v*). The dosage of RAP or PTX was both 10 mg/kg. Tumor volumes and body weights were measured every one day. Tumor volume was calculated by the following formula: $V = 1/2 \times$ (Length) $\times$ (Width)^2. Relative body weight was calculated as follow: Relative body weight $=$ Body weight/Primary body weight.

At day 18, blood was collected from the orbital sinus, and white blood cells (WBC), neutrophils (GRN) and platelets (PLT) were counted to assess the myelosuppressive toxicity in each administration group. At day 20, all animals were sacrificed, and tumors and livers were then dissected. The excised tumors were weighed and pictured to assess the *in vivo* antitumor efficacy. Afterwards, frozen sections made by tumor tissues from each group were stained with TUNEL *in situ* cell death detection kit or treated with TfR antibody (PE labeled-mouse antihuman CD71 antibody), followed by imaged with CLSM. Meanwhile, the other tumor tissues from each group were fixed to evaluate the apoptosis and autophagy of tumor cells by TEM. Lastly, paraffin section made by excised livers were subjected to H&E staining, observed by light microscope to evaluate the organ toxicity.

2.9. Statistical analysis

All quantitative results are reported as mean $\pm$ standard deviation of the mean (SD) unless otherwise specified. Statistical significance was analyzed using two-tailed Student's *t*-test or one-way analysis of variance (ANOVA) followed by a Tukey-Kramer multiple comparison test. A *P*-value less than 0.05 is considered statistically significant, while *P* less than 0.01 was considered highly significant.

3. Results and discussion

3.1. Preparation and characterization of transferrin receptor-targeted micelles

3.1.1. Synthesis of 7peptide conjugated PEG-DSPE polymer
7pep was conjugated to the distal end of PEG through a nucleophilic substitution reaction (Supporting Information Scheme S1). As shown in Supporting Information Fig. S1, the retention time for 7pep monitored by RP-HPLC with gradient elution was around 8.5 min. The peak of 7pep almost disappeared after 120 h reaction, indicating that 7pep had been successfully linked with NHS-PEG-DSPE. As displayed in Supporting Information Fig. S2, there was a strong absorption peak of 7pep at around 281 nm in the UV spectrum of 7pep-PEG-DSPE, while no such peak was observed for NHS-PEG-DSPE, suggesting that 7pep was successfully conjugated to NHS-PEG-DSPE. Moreover, the molecular weight (MW) of final product determined by MALDI-TOF MS was in accordance with theoretical MW (Supporting Information Fig. S3).

3.1.2. Characterization of 7pep-M-RAP and 7pep-M-PTX
The physical properties of micelles are listed in Table 1. All types of nanocarriers are about 15 nm in diameter with PDI less than 0.2, and negatively charged. The TEM images showed that both 7pep-M-RAP and 7pep-M-PTX were spherical in shape and about 15 nm with a narrow distribution, which were consistent with the results determined by DLS (Fig. 1A and B, Supporting Information Figs. S4 and S5). The entrapment efficiencies (EEs) of both RAP and PTX formulations were consistently greater than 90%. There was no obvious difference in physical properties between modified and non-modified nanocarriers, which was favorable for their following comparison *in vitro* and *in vivo* tests. Besides, the experiment of dilution stability revealed that drug-loaded micelles were resistant to about 100 times dilutions (Supporting Information Table S1).

Fig. 1C displays the XRD patterns of RAP powder, blank micelles, physical mixture of RAP plus blank micelles, and lyophilized RAP-loaded micelles, respectively. RAP powder displayed a series of distinct sharp peaks, and similar characteristic peaks of RAP were also observed in the physical mixture of RAP and blank micelles. While no crystal peaks of RAP were seen in the profiles of both RAP-loaded micelles and blank micelles. Similarly, the XRD spectra of PTX-loaded micelles exhibited showed no diffraction peaks assigned to PTX powder (Supporting Information Fig. S6), implying that both RAP and PTX might exist as amorphous or molecular state in their polymeric micelles.

Table 1 Characteristics of various drug-loaded micelles.

Formulation	Size (nm)	PDI	Zeta potential (mV)	EE (%)
Blank-M	14.66 ± 1.23	0.110 ± 0.035	−4.63 ± 1.08	−
Blank-7pep-M	14.01 ± 1.78	0.143 ± 0.041	−4.25 ± 0.97	−
M-RAP	15.31 ± 1.11	0.109 ± 0.099	−4.51 ± 0.78	94.0 ± 4.2
7pep-M-RAP	15.55 ± 1.48	0.150 ± 0.065	−4.28 ± 0.31	95.1 ± 4.3
M-PTX	15.91 ± 1.94	0.134 ± 0.066	−4.32 ± 0.66	94.2 ± 5.4
7pep-M-PTX	16.70 ± 1.34	0.104 ± 0.085	−4.69 ± 0.29	90.1 ± 4.3

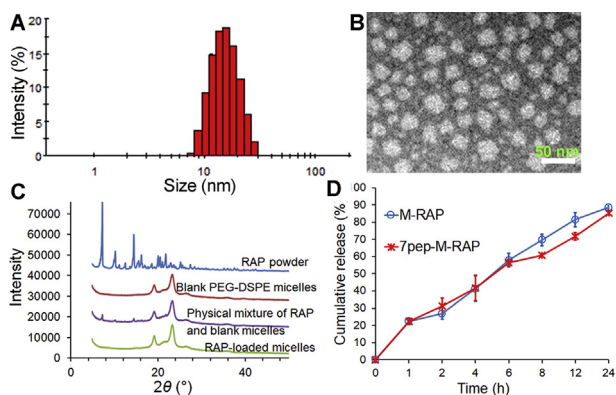− Not applicable. Data are mean ± SD, $n = 3$.

Figure 1 The characteristics of 7pep-modified nanomedicines. (A) Particle size distribution of 7pep-M-RAP. (B) Morphology of 7pep-M-RAP by TEM. (C) Powder X-ray diffraction patterns of various RAP preparations, including RAP powder, blank PMs, physical mixture of RAP plus blank PMs, and lyophilized RAP-loaded micelles. (D) *In vitro* release of RAP and from micelles in 1.0 mol/L sodium salicylate at 37 °C (mean $\pm$ SD, $n = 3$).

Moreover, the CMCs of PEG-DSPE and 7pep-PEG-DSPE were 2.425 and 2.567 μg/mL, respectively, which were close to the previously reported values[33], and were low enough to maintain the micelle state for the materials during the experimental processes. The *in vitro* release of RAP and PTX from micelles 1.0 mol/L sodium salicylate is presented in Fig. 1D and Supporting Information Fig. S7. No burst release was observed, and similar kinetics was observed between 7pep-modified and non-modified micelles.

3.2. Active targeting effect of 7pep-modified-micelles in vitro

Firstly, the TfR expression in human breast-cancer cell line MCF-7 was confirmed by flow cytometry. Supporting Information Fig. S8 shows the plots of MCF-7 cells after incubation with TfR antibody, indicating that the TfR was obviously expressed in MCF-7 cells.

In order to investigate the targeting efficiency of 7pep modification on the micelle internalization, C6-loaded micelles modified with different densities of 7pep were prepared to trace the cellular uptake of PMs. As seen in Supporting Information Fig. S9, the cellular uptake of 7pep-M-C6 was much higher than that of M-C6, and the amount of its accumulation in MCF-7 cells increased with the modification density of 7pep. Given this, micelles modified with 15% of 7pep were constructed for further experiments. The results of receptor competitive experiment showed in Fig. 2A and Supporting Information Fig. S10 revealed that the enhanced cellular uptake by 7pep modification was obviously decreased in the presence of excess antibody, suggesting that the enhanced cellular uptake was probably mediated by the existence of TfR on MCF-7 cells.

Confocal microscope images (Fig. 2B) further verified the results from flow cytometry. The intracellular fluorescence intensity in the 7pep-M-C6 group was greater than that of M-C6, and highly reduced by saturation of TfR. Intracellular distribution study was performed to validate the targeting efficiency of 7pep-M-C6. Fig. 2C and D manifested that 7pep-M-C6 colocalized more with lysosomes than M-C6 after being incubated with MCF-7 cells for 2 h. The different lysosomal distribution characteristics between 7pep-M-C6 and M-C6 revealed that the 7pep modification facilitated the faster and more internalization of micelles into cells[34]. It is worth mentioning that, because of this phenomenon of receptor saturation, the two active targeting nanomedicines which
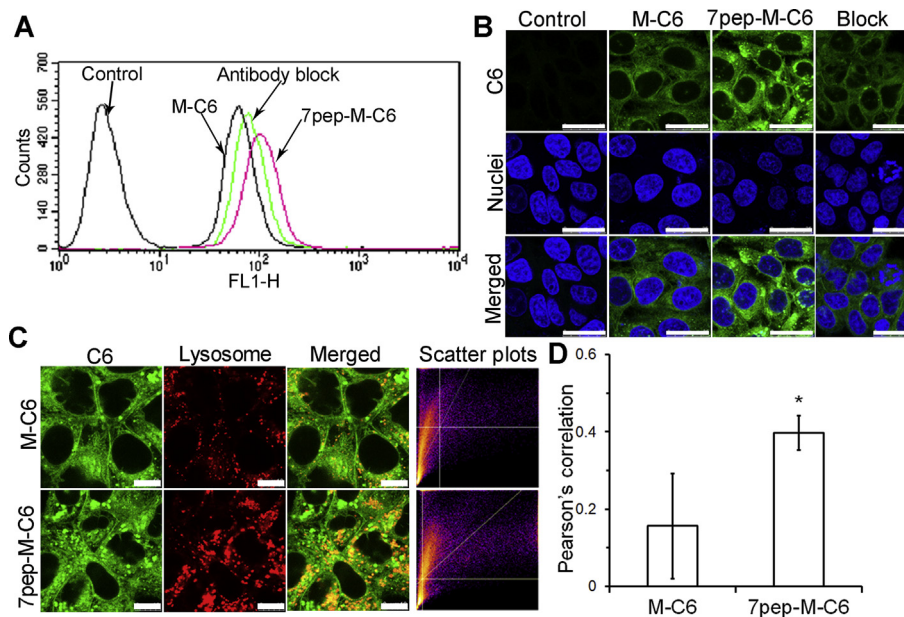

Figure 2 *In vitro* 7pep targeting efficiency in MCF-7 cells. (A) The competitive cellular uptake of various C6 formulations by flow cytometry. MCF-7 cells were incubated with M-C6 or 7pep-M-C6 at a final concentration of 100 ng/mL for 2 h at 37 °C. For receptor competitive experiment, excess anti-TfR antibody was added 0.5 h prior to the 7pep-M-C6. (B) Confocal microscopy images of MCF-7 cells after incubation with M-C6 or 7pep-M-C6 for 2 h at 37 °C. Green and blue represent the fluorescence of C6 and Hoechst 33258, respectively. The white scale bars represent 25 μm. (C) CLSM Images of colocalization of lysosomes (red) with C6-loaded micelles (green). The white bar scales represent 10 μm. (D) Quantitative colocalization analysis of micelles with lysosomes (mean $\pm$ SD, $n = 6$). *$P < 0.05$ *vs* M-C6.

separately encapsulated RAP and PTX might have a competitive inhibitory effect on cellular uptake when administered simultaneously. Therefore, we used HPLC method to investigate the cellular uptake of PTX micelles and RAP-loaded micelles added at the same time point or at certain intervals, thus determining the optimal dosing regimen for the combined administration. The results displayed in Supporting Information Fig. S11 verified our inferences. Based on this, we suggested that RAP and PTX formulations could be administered at certain intervals in following experiments, thus avoiding mutual inhibition of endocytosis.

Totally, the above quantitative and qualitative results consistently demonstrated that the 7pep-modified nanocarriers could increase the delivery to TfR-overexpressing cells *via* a receptor-mediated endocytosis mechanism.

3.3. Superior autophagy induction and synergistic chemotherapy of 7pep-M-RAP

3.3.1. Active autophagy modulation of 7pep-M-RAP

After verified the active targeting efficacy of 7pep-M, we then studied the autophagy inducing ability of 7pep-M-RAP alone or combination with 7pep-M-PTX. The autophagic vesicular accumulation in MCF-7 cells was characterized by the detection of autophagy marker protein LC3B maturation/aggregation, the ratios of LC3-II to LC3-I expression, MDC, as well as Cyto-ID® autophagy detection kit. First, we investigated the effect of different treatments on the maturation/aggregation of LC3B protein by ELISA, which is produced during autophagosome formation and indicates the initiation of autophagy. As demonstrated in Fig. 3A, compared with control and PTX formulation groups, the quantity of LC3B obviously increased in MCF-7 cells treated with RAP formulations in single or combination use. During the formation of autophagosomes, the cytosolic LC3-I protein is activated by Atg7, and then transferred to Atg3, becoming a membrane-bound form LC3- II protein which is located on the autophagosome membranes. Thus, we further measured the conversion of LC3-I to LC3-II by immunoblot (Fig. 3B). Compared with control, the ratios of LC3-II to LC3-I in both 7pep-M-RAP group and combination group increased obviously ($P < 0.05$), but there was no significant difference between these two groups ($P > 0.05$). Then, the colocalization of the LC3B-labeled autophagic vesicles and lysosomes was observed by CLSM to monitor the formation of autolysosomes which are produced during the last stage of autophagy. The fluorescent images and semi-quantitative results in Fig. 3C revealed that both 7pep-M-RAP used alone and in combination caused aggregation of green labeled LC3B protein and higher colocalization rate than control and 7pep-M-PTX monotherapy group. Furthermore, MDC is a tracer for autophagic vacuoles, and the incorporation of MDC into MCF-7 cells was observed with fluorescence microscopy. As shown in Supporting Information Fig. S12, MCF-7 cells treated with 7pep-M-RAP alone or in combination with 7pep-M-PTX demonstrated a punctate pattern of MDC-labeled fluorescence. By contrast, cells in other groups exhibited a diffused distribution of MDC-labeled fluorescence. Cyto-ID is a novel dye that selectively labels autophagic vacuoles and monitors autophagic flux in live cells. As can be seen from Fig. 3D, there is almost no autophagic vesicle in the control group. In contrast, different RAP formulations used in single or in combination induced a large number of green spots of autophagic vesicles. Only a small amount of autophagic vesicles was induced by free PTX alone. This may be

due to the fact that the free drug is highly lipophilic and easily diffuses into MCF-7 cells through the cell membrane, leading to strong cytotoxicity, which resulted in adaptive autophagy for damage caused by chemotherapeutic drug.

In a word, these observations obtained from different methods consistently proved that 7pep-M-RAP could induce significantly more accumulation of autophagic vesicles than M-RAP as well as different PTX formulations. What's more, combination with PTX did not hinder the autophagy induction of 7pep-M-RAP.

3.3.2. Satisfactory synergistic chemotherapy with PTX

After verified the autophagy initiation effect of 7pep-M-RAP, we then investigated the synergy effect with chemotherapy. As exhibited in Supporting Information Figs. S13 and S14, both RAP and PTX preparations inhibited cell proliferation in a dose-dependent manner. Compared with non-modified nanocarriers, 7pep-modified micelles exhibited significantly higher inhibition and much lower IC_{50} value (Table 2). These findings suggested that 7pep modification enhanced the anti-tumor activity *in vitro*, which was in accordance with cellular uptake studies.

It is worth mentioning that, when combined free drugs were administrated simultaneously or free RAP was administered after PTX, no synergistic anti-tumor effect was observed (data not shown), while the scheme that free RAP was administered 12 h prior to PTX showed synergistic effect. This observation indicated that the suitable administration schedule and sequence are very crucial for the therapeutic outcome of combination therapy. Therefore, in conjunction with the results of cell uptake studies, the follow-up studies were conducted with regimen that RAP formulations were applied prior to the PTX. Besides, the *in vitro* cytotoxicity assay revealed that cell viability rates in the combination groups with molar ratio of 1:10 for PTX and RAP was lower than those in groups with concentration ratios of 1:1 or 1:5 (data not shown). The growth inhibition experiment of RAP monotherapy found that MCF-7 cells are less sensitive to low-dose RAP but more sensitive to high-dose RAP treatments. Hence, the concentration ratio of RAP formulations to PTX formulations was set at 10:1 (mol/mol) to achieve better cytotoxicity. The relative dose–effect curve is presented in Fig. 4A. Sequential administration of 7pep-M-PTX after 7pep-M-RAP led to greater proliferation suppression of tumor cells than 7pep-M-PTX used in single. The combination therapy of 7pep-M-RAP and 7pep-M-PTX achieved better inhibitory effect than combined use of M-RAP and M-PTX (Supporting Information Fig. S15). Additionally, the relevant IC_{50} and CI_{50} values of two drugs combined are summarized in Table 2 and Fig. 4B. The IC_{50} of each nanomedicine in combination group exhibited lower values compared with that of single drug group, implying that the co-administration strategy improved the cytotoxic sensitivity towards MCF-7 cells. The CI_{50} values of the three combination groups ($CI_{50} = 0.362$, 0.511 and 0.546 for Free Combi, M-Combi, and 7pep-M-Combi, respectively) were all below 0.90, further demonstrating the synergy effect of RAP and PTX in MCF-7 cells.

Annexin V-FITC/PI apoptosis detections were utilized to further verify the synergy effects of combinational treatments on MCF-7 cells. Qualitative and quantitative results are displayed in Fig. 4C and Supporting Information Fig. S16, respectively. Compared with control group, the blank 7pep-modified micelles did not induce obvious apoptosis of MCF-7 cell, indicating the biocompatibility of micellar polymers. Both combination groups induced a higher proportion of apoptosis than either RAP or PTX preparations used alone, whereas the combination of 7pep-
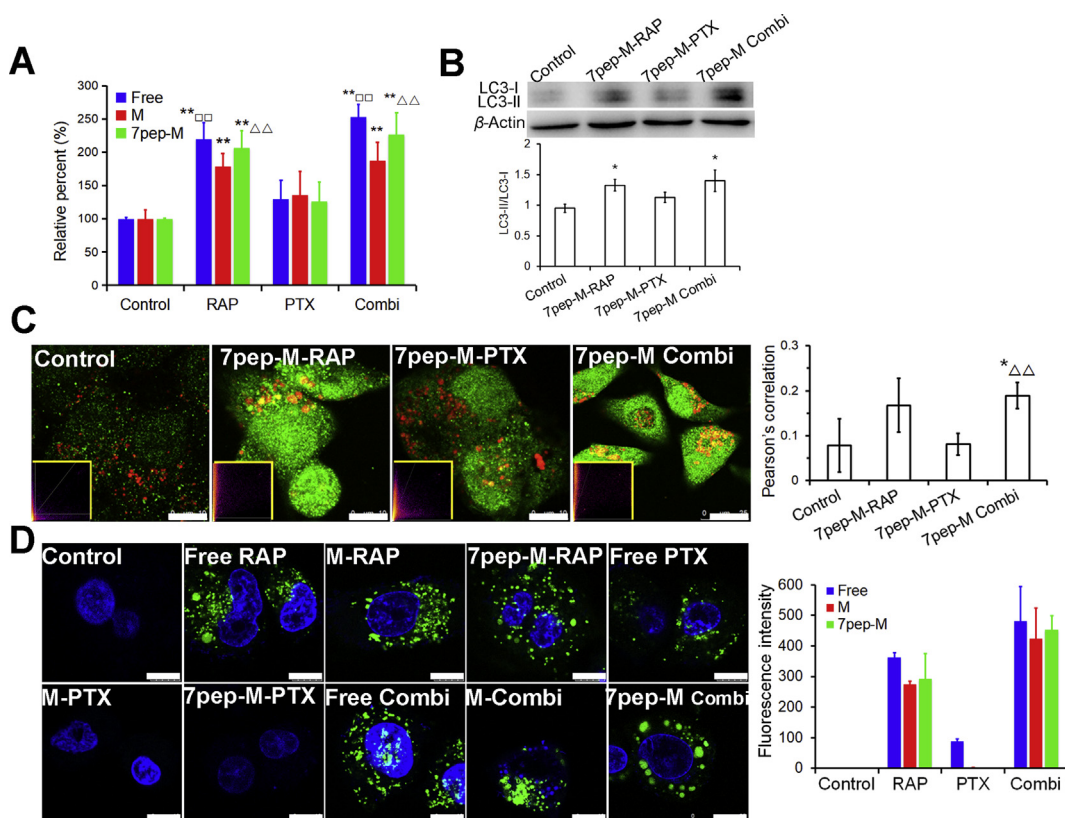
Figure 3 Active autophagy modulation of 7pep-M-RAP. (A) Quantitative analysis of cellular LC3B by ELISA assay (mean ± SD, $n = 3$). $^{**}P < 0.01$ vs Control; $^{\square\square}P < 0.01$ vs Free PTX; $^{\triangle\triangle}P < 0.01$ vs 7pep-M-PTX. (B) Effects of different treatments with nanomedicines on the ratios of LC3-II to LC3-I. Levels of LC3B proteins expression were measured by western-blot, and the ratios of LC3-II to LC3-I were calculated by comparing the band densities (mean ± SD, $n = 3$). $^*P < 0.05$ vs Control. (C) Images and quantitative analysis of colocalization of the LC3B-labeled autophagic vesicles (green dots) and Lyso-tracker red-labeled lysosomes (red). The white scales represent 10 μm. Yellow-framed inserts show the scatter plots generated by Image J software (mean ± SD, $n = 6$). $^*P < 0.05$ vs Control; $^{\triangle\triangle}P < 0.01$ vs 7pep-M-PTX. (D) Images and quantitative analysis of autophagic vacuoles specifically labeled by Cyto-ID dye (green). The cell nuclei were stained with Hoechst 33342 (blue). The white scales represent 10 μm. Each bar on the histogram represents mean fluorescence intensity obtained from 6 randomly selected cells (mean ± SD, $n = 6$).

modified nanocarriers (42.89%) prompted more apoptosis than non-modified micelles (31.00%). These observations were consistent with the results of cytotoxicity *in vitro*. Moreover, neither RAP formulations used alone induced obvious apoptosis, manifesting that RAP might not play a role of apoptosis inducer in the synergy effects of combination groups.

3.4. Mechanism of the improved therapeutic efficacy of combination therapy

3.4.1. Autophagy inhibitor 3-MA suppressed the cytotoxicity and autophagic vesicular accumulation of combination therapy
Then, we explored the underlying mechanism for this synergy effect of 7pep-M-RAP combined with 7pep-M-PTX for breast

Table 2 IC$_{50}$ values and CI$_{50}$ values of RAP and PTX for different formulations used in single or in combination.

Formulation	IC$_{50}$ of PTX (nmol/L)[a]	IC$_{50}$ of RAP (μmol/L)[a]	CI$_{50}$
Free drug	7.93 ± 0.34	48.08 ± 4.37	−
PM monotherapy	16.73 ± 0.69	64.95 ± 4.15	−
7pep-M monotherapy	9.32 ± 0.48	55.73 ± 4.22	−
Free Combi	4.86 ± 0.21	0.0286 ± 0.0015	0.362
M-Combi	8.52 ± 0.40	0.0852 ± 0.0066	0.511
7pep-M-Combi	5.08 ± 0.35	0.0508 ± 0.0058	0.546

− Not applicable.
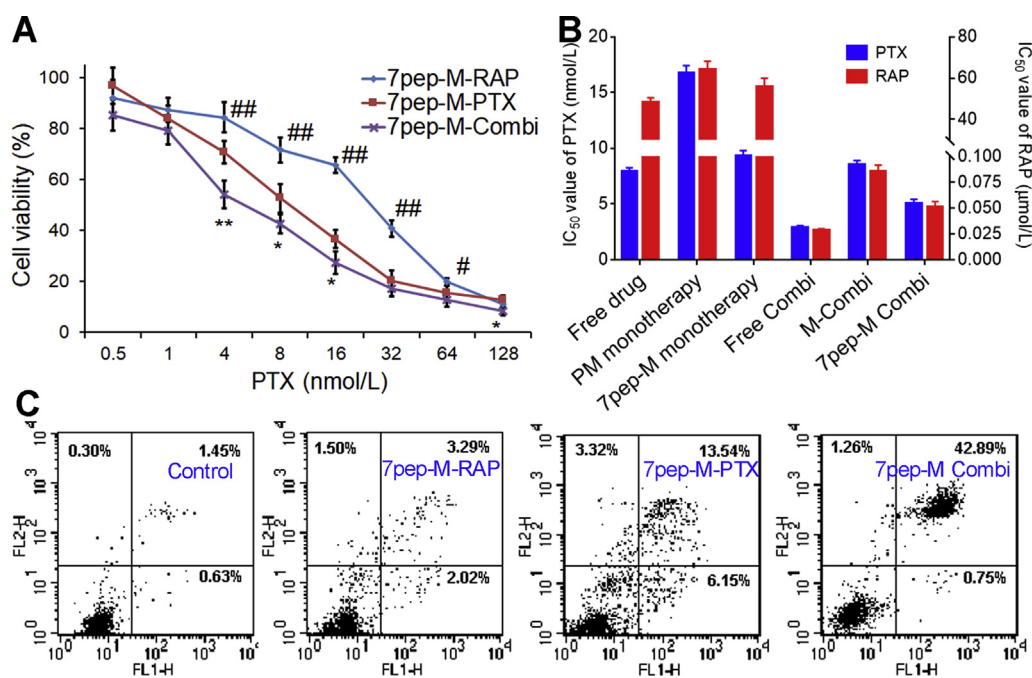[a]Data are mean ± SD, $n = 6$.

Figure 4 Satisfactory synergistic chemotherapy with PTX. (A) Cytotoxicity of 7pep-M-Combi compared with 7pep-M-PTX or 7pep-M-RAP in single use (mean ± SD, $n = 6$). $^*P < 0.05$ and $^{**}P < 0.01$, 7pep-M-PTX vs 7pep-M-Combi; $^\#P < 0.05$ and $^{\#\#}P < 0.01$, 7pep-M-RAP vs 7pep-M-Combi. (B) IC_{50} values of RAP and PTX for different formulations used in single or in combination. (C) *In vitro* cell apoptosis evaluation of micelles against MCF-7 cells by flow cytometry. Double parameter dot plots show FITC-fluorescence (FL1-H axis) vs PI-fluorescence (FL2-H axis). Quadrants: lower left, normal live cells (annexin V$^-$/PI$^-$); lower right, early apoptotic cell (annexin V$^+$/PI$^-$); upper right, late apoptotic or necrotic cells (annexin V$^+$/PI$^+$); and upper left, mechanically injured cells (annexin V$^-$/PI$^+$).

cancer. Since 7pep-M-RAP could actively trigger autophagy as proved above, we assumed that excessive autophagy induced by high concentrations of RAP would cause damage to intracellular mitochondria or other organelles, and this effect, together with apoptosis induced by PTX, plays a role in promoting tumor cell death. In order to verify the above hypothesis, autophagy inhibitor 3-MA was involved to evaluate the relevance between autophagy and anti-tumor effect. Furthermore, mitochondrial morphology, mitochondrial membrane potential, cytochrome C release, intracellular ATP content, and the activities of caspase-9 and 3 were investigated to examine the effect of co-administration induced autophagy on the morphology and function of mitochondria.

As depicted in Fig. 5A and B, as well as Supporting Information Figs. S17 and S18, the cell viability of 7pep-M-PTX monotherapy, combination group, and combination therapy plus 3-MA were 50.53 ± 4.04%, 30.67 ± 4.61%, 40.54 ± 4.13%, respectively, and the apoptosis proportion in above three treatment groups were 15.5 ± 4.14%, 45.94 ± 3.33%, 37.12 ± 4.84%, respectively. The results of SRB cytotoxicity assay and annexin V-FITC/PI apoptosis analysis consistently demonstrated that the combination use of 7pep-M-RAP and 7pep-M-PTX enhanced the chemosensitivity to 7pep-M-PTX in TfR-overexpressing breast cancer cells, and this synergistic interaction were significantly suppressed by autophagy inhibitor 3-MA ($P < 0.05$), suggesting that 7pep-M-RAP-induced autophagy might play an active role in enhanced anti-tumor effect.

Cyto-ID® autophagy detection and LC3B protein aggregation determination were also applied to further confirm whether the synergism induced by the combination treatment involved the active autophagy modulation effect of 7pep-M-RAP. Qualitative and quantitative analysis of Cyto-ID staining further verified that 7pep-M-RAP alone or in combination with 7pep-M-PTX could induce similar levels of autophagic vesicle accumulation, while 3-MA could effectively inhibit the autophagic vacuoles accumulation (Fig. 5C and D). Moreover, with the addition of 3-MA, the ratios of LC3-II to LC3-I expression, fluorescence dots of LC3B aggregation, and the quantity of LC3B measured by ELISA consistently decreased significantly both in single 7pep-M-RAP and combination group (Fig. 5E and F, and Supporting Information Fig. S19).

Therefore, we came to a preliminary conclusion that the autophagy induced by 7pep-M-RAP played an important role in the synergistic effect of combination therapy. It is worth noting that 3-MA could not completely reverse the efficacy of co-administration, indicating that autophagy is one of the many mechanisms for the synergy between 7pep-M-RAP and 7pep-M-PTX. The currently reported synergistic anti-tumor mechanisms of combined RAP (or its derivatives) with PTX mainly involves the anti-angiogenesis effect of RAP and its direct inhibition of mTOR in tumor development[11,13,35]. It was reported that PTX down-regulates Akt phosphorylation followed by mTOR activation, which promotes resistance to chemotherapy and hormone therapies in breast cancer cells, while RAP blocks the phosphoinositide 3-kinase (PI3K)/AKT/mTOR/p70S6K pathway, thus reversing drug resistance[36–38]. Besides, the inhibition of mTOR arrests the cells cycle in G1 phase, while PTX leads to G2/M phase arrest, this dual role leads to synergy effects[15]. However, the relationship between autophagy and synergistic effect of this combined strategy is not well understood. Therefore, our research attempted to clarify the role of RAP-induced autophagy in the combined anti-tumor efficacy.
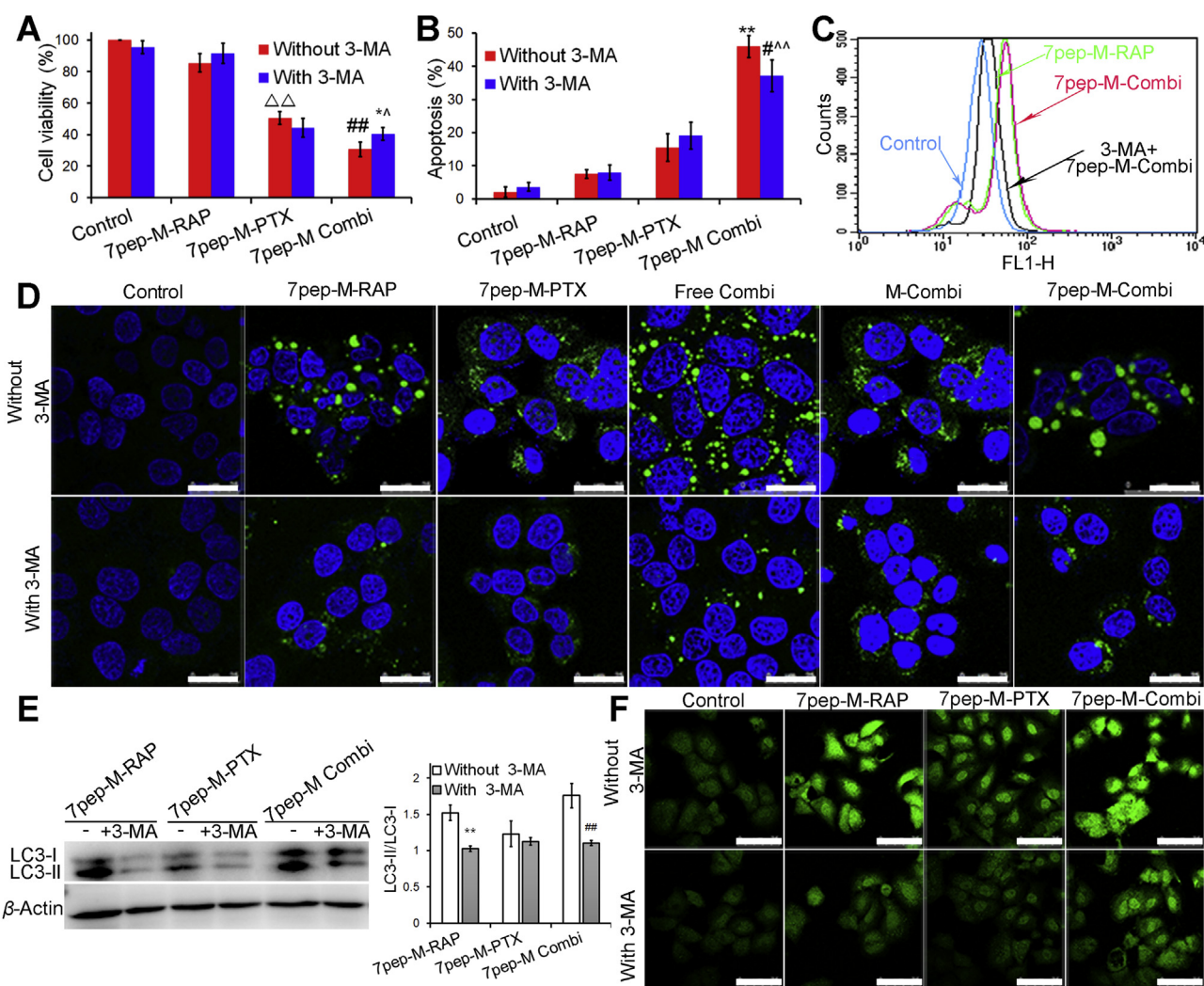
Figure 5 The inhibition effect of autophagy inhibitor 3-MA on cytotoxicity, apoptosis and intracellular autophagic vesicular accumulation. (A) The effect of 3-MA on the cytotoxicity induced by 7pep-M-PTX in single or in combination with 7pep-M-RAP (mean ± SD, $n = 6$). $^{\triangle \triangle}P < 0.01$ vs control without 3-MA; $^{\#\#}P < 0.01$ vs 7pep-M-PTX without 3-MA; $^{*}P < 0.05$ vs 7pep-M-Combi without 3-MA; $^{\wedge}P < 0.05$ vs 7pep-M-PTX without 3-MA. (B) Quantitative analysis of in vitro cell apoptosis based on flow cytometric plots (mean ± SD, $n = 4$). Each bar represents the sum of early apoptotic cells and late apoptotic cells. $^{**}P < 0.01$ vs 7pep-M-PTX without 3-MA; $^{\#}P < 0.05$ vs 7pep-M-Combi without 3-MA; $^{\wedge}P < 0.01$ vs 7pep-M-PTX without 3-MA. (C) The effect of 3-MA on the Cyto-ID specifically labeled autophagic vesicles detected by flow cytometry. (D) The inhibition effect of 3-MA on the Cyto-ID dye specifically labeled autophagic compartments. Images showed the colocalization of the Cyto-ID fluorescence dye (green) and Hoechst 33342 (blue). The white scales represent 25 μm. (E) Levels of LC3-II to LC3-I measured by western-blot, and the ratios of LC3-II to LC3-I were calculated by comparing the band densities (mean ± SD, $n = 3$). $^{**}P < 0.01$ vs Control. $^{\#\#}P < 0.01$ vs 7pep-M Combi without 3-MA. (F) The inhibition effect of 3-MA on the LC3B labeled autophagic vesicles. The white scale bars represent 75 μm.

3.4.2. Effect of co-administration induced autophagy on the morphology and function of mitochondria

To further assess the effect of co-administration induced autophagy on intracellular organelles, we examined the morphology and function of mitochondria, including TEM, co-localization of mitochondria with autophagic vesicles, change in MMP, release of cytochrome C, intracellular ATP levels, as well as activities of caspases 9 and 3.

From TEM images in Fig. 6A and quantitative analysis results in Supporting Information Fig. S20, apoptotic body was observed in MCF-7 cells exposed to 7pep-M-PTX alone, confirming the presence of apoptotic cell death. In contrast, MCF-7 cells treated

with 7pep-M-RAP alone or in combination with 7pep-M-PTX, contained a number of autophagic vacuoles, with digested materials or dysfunctional mitochondria that were sequestered into a double-membrane-bound vesicle and lost their crista. Mitochondria were abnormal in appearance and an increased number of lysosomes were also observed. Consistent with the results obtained under an electron microscope, the confocal microscopy revealed that the combination of 7pep-M-RAP and 7pep-M-PTX resulted in higher co-localization rate of Cyto-ID specifically labeled-autophagic vesicles with Mitotracker labeled-mitochondria compared with monotherapy groups (Fig. 6B and Supporting Information Fig. S21). With the addition of 3-MA,
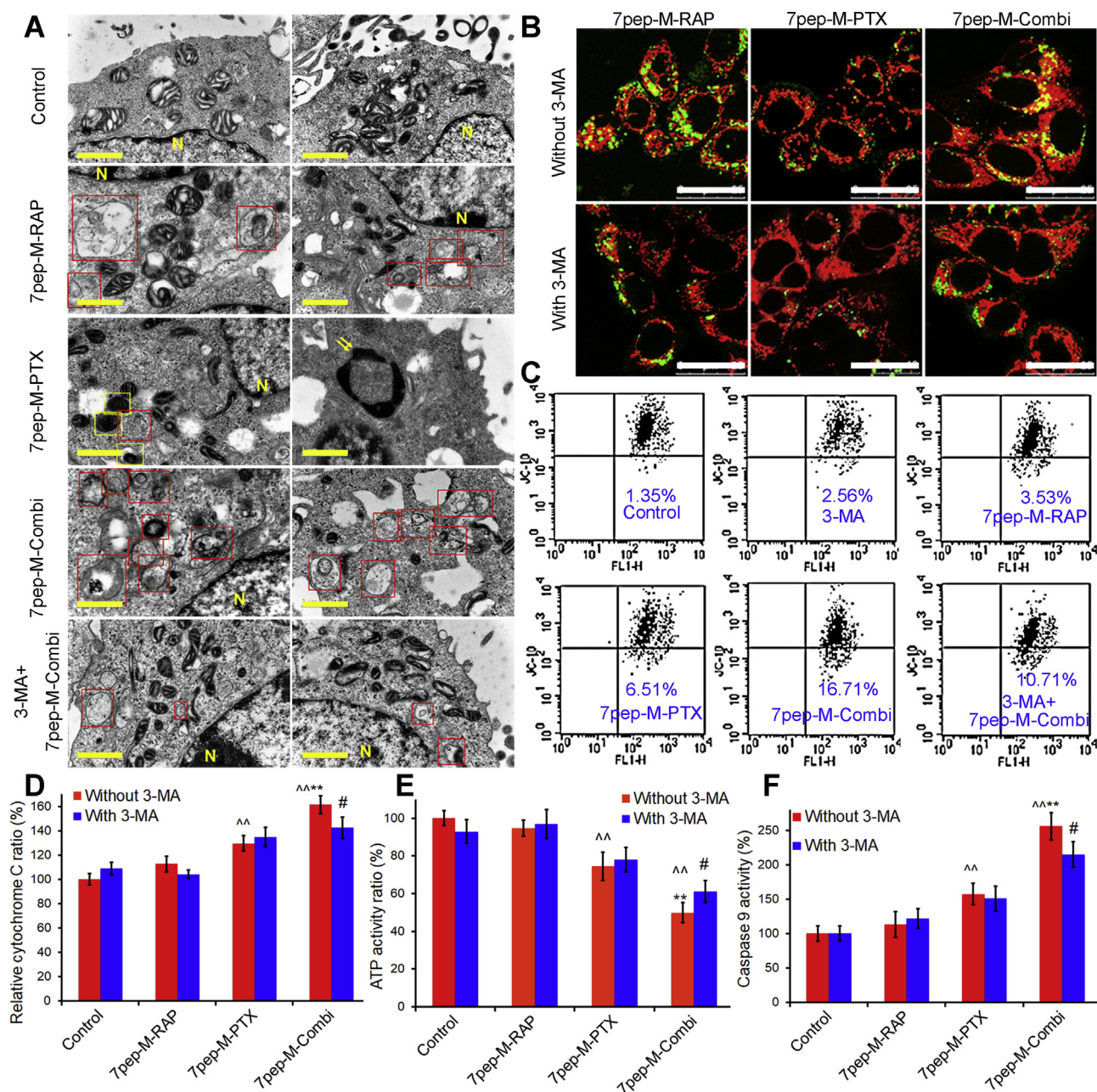
Figure 6 Effect of co-administration induced autophagy on the morphology and function of mitochondria. (A) TEM micrographs of MCF-7 cells untreated (control) or treated with 7pep-M-PTX, 7pep-M-PTX, 7pep-M-Combi and 3-MA plus 7pep-M-Combi. Nucleus (yellow letter N), typical autophagosomes (red frames), damaged mitochondria (yellow frames) and apoptotic body (yellow arrows) are indicated. The yellow scales represent 1.0 μm. (B) Images and quantitative analysis of colocalization (yellow dots) of Cyto-ID specifically labeled autophagic vesicles (green dots) and Mitotracker labeled mitochondria (red) in MCF-7 cells treated without or with 3-MA. The white scales represent 25 μm. (C) Decline of mitochondria membrane potential ($\Delta\psi$) measured by flow cytometry. Live MCF-7 cells were stained with JC-10 after exposed to various formulations. (D) Quantitative analysis of cellular cytochrome C by ELISA assay (mean ± SD, $n = 3$). $^{\wedge}P < 0.01$ vs Control; $^{**}P < 0.01$ vs 7pep-M-PTX without 3-MA; $^{\#}P < 0.05$ vs 7pep-M-Combi without 3-MA. (E) Quantitative analysis of cellular ATP measured by luminometer (mean ± SD, $n = 3$). $^{\wedge}P < 0.01$ vs Control; $^{**}P < 0.01$ vs 7pep-M-PTX without 3-MA; $^{\#}P < 0.05$ vs 7pep-M-PTX with 3-MA. (F) Activity of caspase-9 in MCF-7 cells induced by various formulations (mean ± SD, $n = 3$). $^{\wedge}P < 0.01$ vs Control; $^{**}P < 0.01$ vs 7pep-M-PTX without 3-MA; $^{\#}P < 0.05$ vs 7pep-M-Combi without 3-MA.

both the accumulation of autophagic vesicles and co-localization of mitochondria with autophagic vesicles in combined therapy group were reduced and the number of mitochondria was increased. This might be due to the down-regulation of autophagy by 3-MA and the reduction of mitophagy. Selective degradation of

mitochondria by autophagy is also known as 'mitophagy' and is considered to be promoted by their functional impairment and/or by MMP. Mitophagy may ensure the removal of damaged and potentially dangerous mitochondria, while excessive autophagy may cause damage to the function of organelles[39−41]. Since

decline in MMP is a morphological characteristic of mitochondrial function recession, we then used JC-10 to detect the changes in MMP by flow cytometry and confocal analysis. JC-10 is a cationic lipophilic fluorescent dye. It accumulates in mitochondria and its intake is proportional to the MMP. As indicated in Fig. 6C and Supporting Information Fig. S22, the fluorescence intensity of JC-10 was obviously lower in the cells exposed to 7pep-M-RAP in combination with 7pep-M-PTX relative to the other groups, while the fluorescence intensity increased with the pretreatment of 3-MA, suggesting that the decrease of MMP induced by co-administration might be related to autophagy.

Fig. 6D and F, as well as Supporting Information Fig. S23 present the change in function of mitochondria with different treatments. It was showed that when compared with monotherapy, 7pep-M-RAP plus 7pep-M-PTX induced increased release of cytochrome *c* from mitochondria (Fig. 6D), decreased intracellular ATP content (Fig. 6E), as well as enhanced activities of caspase-9 and -3 (Fig. 6F and Supporting Information Fig. S23), and these effects could be partly suppressed by 3-MA. These findings showed that the mitochondrial morphology and function were impaired by the combination therapy, and this effect on mitochondria might be partially associated with 7pep-M-RAP-induced autophagy.

Mitochondria are vital organelles for cellular metabolism and bioenergetics of eukaryotic cells, involving a variety of biological processes, such as intracellular homeostasis, cell proliferation, senescence, and death[42]. Based on the above results, it could be speculated that during the combination therapy of 7pep-M-RAP and 7pep-M-PTX, mitophagy occurred in MCF-7 cells, which led to mitochondrial damage, followed by mitochondrial membrane permeability transition, oxidative phosphorylation decoupling, excessive depletion of ATP, and the release of cytochrome c into cytoplasm after mitochondrial swelling[43]. After cytochrome *c* release, caspase 9 was activated by a series of signaling pathways that activated downstream cascade enzymes, such as caspase-3, causing a downstream cascade that eventually triggered apoptosis[44]. In short, it was demonstrated that 7pep-M-RAP enhanced 7pep-M-PTX-induced mitochondria-associated apoptosis at least partly through autophagy activation, thereby enhancing the anti-tumor effect of 7pep-M-PTX.

Studies have shown that RAP at a concentration of greater than 100 nmol/L brought on autophagy-related death in drug-resistant NIH 3T3 cells[45], which is similar to our results on MCF-7 cells in this study. It could be deduced that when 7pep-M-RAP is administered simultaneously with 7pep-M-PTX, or 7pep-M-RAP is administered after 7pep-M-PTX, cytotoxic PTX would firstly cause organelle damage, and then the autophagy induced by RAP might play a role in protecting MCF7 breast cancer cells from organelle damage caused by PTX. On the contrary, the pretreatment with 7pep-M-RAP on MCF-7 cells induced a large number of autophagy, resulting in excessive depletion of key intracellular processes and rapid accumulation of intracellular autophagic vesicles, whereas cells could not degrade the contents in time, leading to abnormal accumulation of autophagosomes and imbalance of cell functions[46,47]. During autophagy development, the non-specific capture of cytoplasmic components led to irreversible damage to mitochondria or other organelles. At this time, the application of cytotoxic chemotherapeutic agents, such as PTX, aggravated the injury of organelles, which eventually led to cell death. Under the circumstances, the intracellular balance was broken, and autophagy no longer played a protective role, but promoted cell death.

In summary, based on our findings, it can be concluded that a combined strategy targeting autophagic cell death has great potential for enhancing the antitumor efficacy of chemotherapeutic agents. However, in view of the biphasic effect of autophagy, there is a requirement to establish the appropriate concentration of rapamycin and sequence of administration that is capable of activating autophagy, inducing mitophagy or promoting tumor cell apoptosis, so as to provide a new approach to treating malignant tumor.

3.5. Targeted delivery of nanomedicines to MCF-7 tumor-bearing nu/nu mice

To further investigate the tumor targeting efficacy of 7pep-modified micelles and optimize the dosage regimen, we applied *in vivo* fluorescence imaging on MCF-7 tumor-bearing mice models. Fig. 7A displays the fluorescence distribution of tumor-bearing nude mice at different time points after the administration of M-DiR or 7pep-M-DiR. For all groups, the fluorescence intensity in the tumor sites increased with time. The DiR accumulation of 7pep-M-DiR at the tumor site was higher than that of M-DiR at all time points. Compared with 7pep-M-DiR group, the fluorescence intensity of 7pep block group at the tumor site was significantly lower at all time points, suggesting that 7pep in blank active micelles could competitively inhibit the distribution in tumors after specifically binding to TfR. This finding indicated that the *in vivo* targeting effect of 7pep-modified micelles was still a receptor-mediated process. From Fig. 7B, the 7pep-M-DiR group showed higher fluorescent intensity in excised tumor than M-DiR group, while no distinct difference was detected in the other main organs.

The bio-distribution of 7pep-M-DiD and 7pep-M-DiR used in combination was further performed to investigate the effect of different dosing regimens on the drug distribution in tumor sites. DiD was employed as the indicator for RAP loaded in 7pep-M-RAP and DiR was applied as the indicator for PTX loaded in 7pep-M-PTX. It has been reported that the two fluorescence probes did not interfere with each other under their respective excitation/emission conditions and could be used simultaneously for tissue distribution studies in combination administration[48]. As the appropriate administration sequencing is very crucial for the therapeutic outcome of combination therapy[48], two different dosing regimens were compared to achieve better distribution characteristics with dual-nanomedicines (Fig. 7C). As shown in Fig. 7D and F, when two nanocarriers were administrated simultaneously (referred to as Combi-simu group), the fluorescence intensity of either DiR or DiD increased over time until the peak at 24−36 h, then decreased till the end of experiment. This tendency of signal intense was similar to that of monotherapy group, indicating that the co-administration had no effect on the peak time and elimination rates of nanomedicines compared with single drug treatments. However, the fluorescence intensity of either DiR or DiD was lower than that of the monotherapy group at the same time point, respectively. This phenomenon in Combi-simu group was particularly pronounced. It could be speculated that the two micellar formulations exhibited the similar peak times and the accumulation process after simultaneous administration, which might lead to competitive penetration into the tumor tissues. In addition, the 7pep modified on 7pep-M-DiD and 7pep-M-DiR competitively binds to TfR in tumor cells, resulting in a competitive uptake of nanocarriers, which were consistent with the observations of *in vitro* cellular uptake. In view of this, we proposed a cross-over design in which DiD-loaded nanocarriers were injected 24 h prior to the injection of DiR-loaded nanocarriers (referred to as Combi-cros
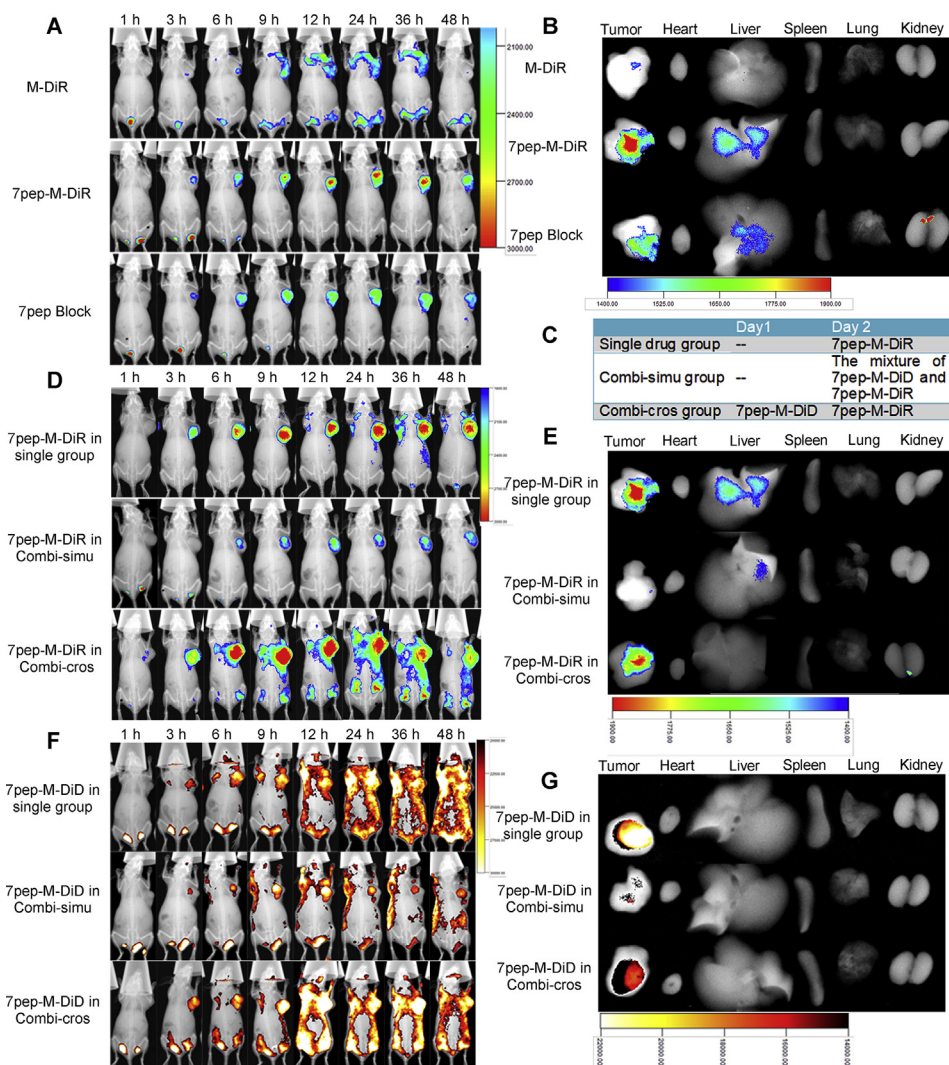
Figure 7 *In vivo* targeted delivery of nanomedicines used in single or in combination to MCF-7 tumor-bearing nu/nu mice. (A) *In vivo* specific delivery of TfR-targeted nanocarriers used alone. Mice were treated with M-DiR, 7pep-M-DiR, or blank 7pep-M plus 7pep-M-DiR (Referred to as 7pep block group, in which mice were injected with 200 μL of blank 7pep-PMs 1 h before administration of 7pep-M-DiR). (B) *Ex vivo* fluorescent images of tumor and major organs. (C) Dosing schemes of 7pep-M-DiD and 7pep-M-DiR for *in vivo* tissue distribution. MCF-7 tumor bearing mice were treated with single 7pep-M-DiR, 7pep-M-DiR plus 7pep-M-DiD administrated simultaneously (Referred to as Combi-simu group), 7pep-M-DiR plus 7pep-M-DiD predosed 24 h prior to 7pep-M-DiR (Referred to as Combi-cros group). (D) and (F) *In vivo* distribution of dual-nanomedicines administrated simultaneously or at certain intervals. The fluorescent images of DiR and DiD are shown in (D) and (F), respectively. (E) and (G) *Ex vivo* fluorescent images of tumor and main organs.

group), aiming to avoid the competitive inhibition effect. As seen in Fig. 7D−G, the accumulation of either DiR or DiD at the tumor sites in Combi-cros group was similar to that of the single drug administration group, which was in line with our expectation.

Based on above findings, it was suggested that the two nanomedicines should be administered at certain intervals to avoid the competitive inhibition caused by simultaneous administration *in vivo* distribution study.

3.6. The combination therapy against the MCF-7 tumor in nude mice

Next, the *in vivo* anti-tumor efficacy of 7pep-M-RAP and 7pep-M-PTX used in single or in combination were investigated in nude mice bearing MCF-7 breast cancer. As seen from tumor growth curves in Supporting Information Figs. S24 and S25, all RAP preparations used alone had weak tumor growth inhibitory effect, and there was no significant difference between different RAP preparations. 7pep-M-PTX monotherapy revealed better anti-tumor effect than both commercial product of PTX and unmodified micelles. It could be speculated that this better tumor suppression effect of 7pep-modified polymer micelles might be contributed to its more accumulation at tumor sites through EPR effect and TfR-mediated endocytosis as proved above. Meanwhile, the expression level of transferrin receptor in excised tumor tissues was confirmed by immunofluorescence. As seen in Supporting Information Fig. S26, obvious red fluorescence was observed around nuclei, suggesting that TfR was highly expressed on MCF-7 cells, which was in accordance with *in vitro* experimental result.
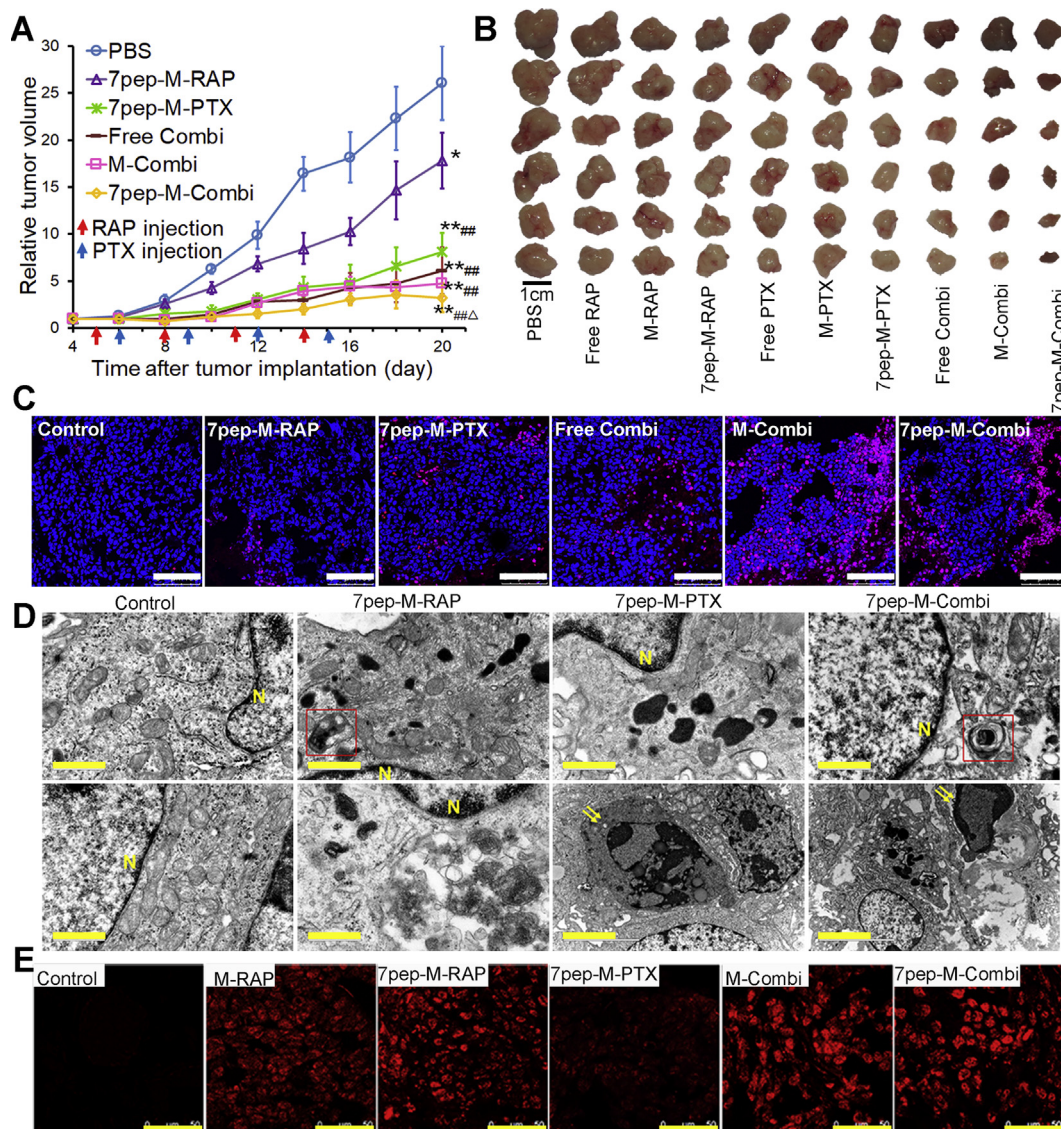
Figure 8 The combination therapy against the MCF-7 tumor in nude mice. (A) Tumor growth curves of mice treated with PBS, 7pep-M-RAP, 7pep-M-PTX, Free Combi, M-Combi or 7pep-M-Combi (mean ± SD, $n = 6$). Arrows indicate the time for injection. $**P < 0.01$ *vs* PBS; $##P < 0.01$ *vs* 7pep-M-RAP; $\triangle P < 0.05$ *vs* 7pep-M-PTX. (B) The photo of excised tumors from different treatment groups. Scale bar = 1 cm. (C) Confocal images of TUNEL assay for apoptotic cells in tumor tissue sections from different treatment groups. DNA strand breaks were labeled with Texas red (red), and nuclei were stained with Hoechst 33258 (blue). Apoptotic cells exhibited the co-localization of these two labels. White scale bars = 100 μm. (D) TEM pictures of tumor masses with different treatments. Nucleus (yellow N), typical autophagosomes (red frames) and apoptotic body (yellow arrows) are indicated. Yellow scale bars = 1.0 μm. (E) Confocal images of LC3B aggregation (red dots) in tumor tissue sections from different treatment groups by immunofluorescence staining. Yellow scale bars = 50 μm.

The all three combined treatment groups exhibited significant enhanced antitumor effects over either RAP or PTX administrated alone at all time points. The antitumor efficacy of three combination groups was found in a descending order as: 7pep-M-Combi > M-Combi > Free Combi (Fig. 8A). The tumor weight measured at the end of test and the image of excised tumors further illustrated the similar observations (Fig. 8B and Supporting Information Fig. S27). These results are in agreement with the tendency of *in vitro* cellular uptake, cytotoxicity, cell apoptosis, as well as *in vivo* drug accumulation in tumors.

In order to explore the mechanism of combined administration, cell apoptosis was detected by TUNEL technique, and the autophagy of tumor cells was examined by TEM and immunofluorescence. As displayed in Fig. 8C–E, as well as Supporting Information Fig. S28, compared with 7pep-M-PTX monotherapy, 7pep-M-RAP used in single induced less cell apoptosis but more autophagic vesicles accumulation in tumor tissue, while the combination of 7pep-M-RAP and 7pep-M-PTX resulted in not only significantly more apoptosis but also higher level of autophagic vesicle accumulation. It is known that RAP is an autophagy inducer, and PTX is an apoptosis inducer that acts on tubulin. The combination of the two nanomedicines led to an increase in apoptosis and autophagy. Based on the *in vitro* findings, it could be speculated that the synergistic effect of 7pep-M-RAP and 7pep-M-PTX might be partly due to ACD induced by RAP and apoptosis induced by PTX.
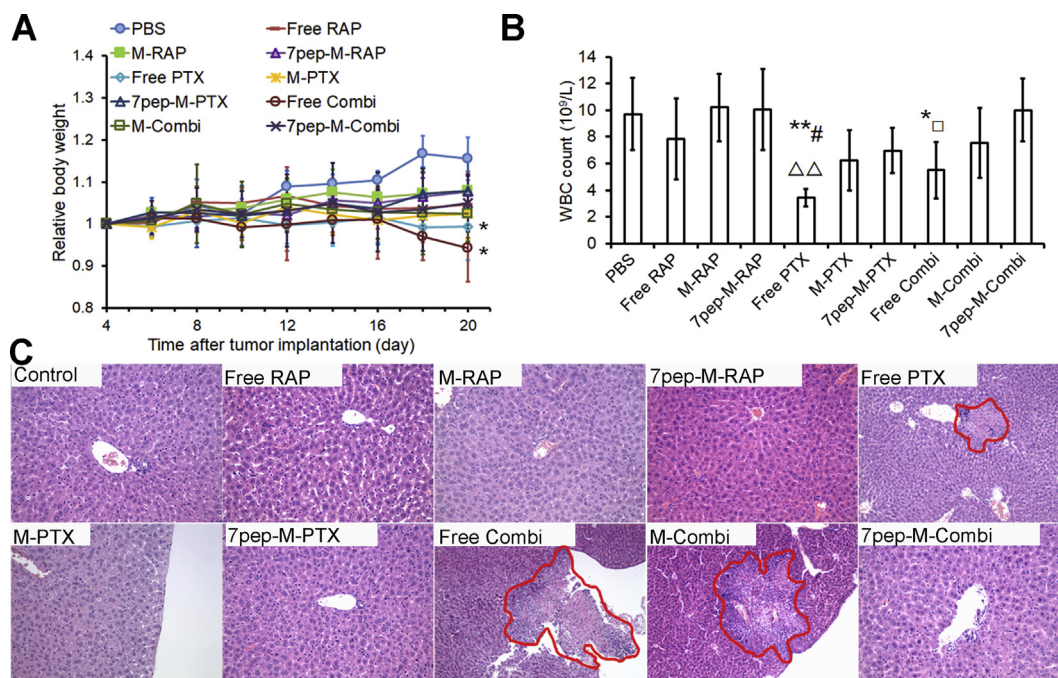
Figure 9 Toxicity studies after intravenous administration. (A) Body weight changes of mice during antitumor efficacy study (mean $\pm$ SD, $n = 6$). Arrows indicate the time for injection after tumor cells inoculation. $^*P < 0.05$ *vs* PBS. (B) Effects of different formulations on white blood cells (WBC) counts at the end of test (mean $\pm$ SD, $n = 5$). $^*P < 0.05$ and $^{**}P < 0.01$ *vs* PBS; $^\#P < 0.05$ *vs* M-PTX; $^{\triangle\triangle}P < 0.01$ *vs* 7pep-M-PTX; $^\square P < 0.05$ *vs* 7pep-M-Combi. (C) Optical microscopy images of H&E staining livers after treated with different formulations. Magnification, $200\times$. Red circles indicate the necrotic area in livers.

3.7. Toxicity studies after intravenous administration

The changes of body weight, leucocyte, neutrophil and platelet count in nude mice after administration were also examined to evaluate the chemotherapy associated toxicity. There was no significant body weight loss for all treated animals except that free PTX group and free drugs combination group showed a decline trend in body weight (Fig. 9A), indicating the acceptable tolerance of different nanomedicines, especially the combinational therapies. As shown in Fig. 9B, as well as Supporting Information Figs. S29 and S30, compared with control group, the combination group of free PTX and free RAP exhibited a significant decrease in WBC, GRN and PLT counts, while nanomedicines combination group only had a minor adverse effect on the blood cells ($P > 0.5$), implying reduced hematotoxicity of chemotherapeutic agents due to the encapsulation in nanocarriers. H&E staining results of excised livers showed that free PTX, Free Combi and M-Combi caused obvious liver necrosis, while no apparent liver toxicity was observed in other groups (Fig. 9C). The safety advantages of nanomedicines were likely due to the lack of haemolytic Cremophor EL and the modification of 7pep on micelles, resulting in less non-specific distribution and greater accumulation at tumor sites, which was in accordance with the tissue distribution results *in vivo*.

Therefore, combinational therapies using 7pep-M-RAP with 7pep-M-PTX could achieve better anti-tumor efficacy with low systemic and hematotoxicity.

4. Conclusions

In summary, our study provides proof-of-concept for 7pep-M-RAP as a novel treatment modality to improve the therapeutic efficacy of chemotherapeutic nanomedicine. 7pep-M-RAP revealed synergistic anti-tumor effect with cytotoxic 7pep-M-PTX on MCF-7 breast cancer. Through ligand–receptor-mediated active targeting and inducing massive accumulation of autophagic vesicles, combination chemotherapy that acted on both ACD and apoptosis provided enhanced efficacy and reduced toxicity. Combined with targeted DDS (7pep-M-PTX) of chemotherapeutic agent, 7pep-M-RAP brought on mitochondria-associated apoptosis and direct tumor suppression. To the best of our knowledge, relevant studies have not reported previously that RAP is prepared as a targeting DDS for inducing ACD. As a result, the combination of autophagy-targeted DDS with cytotoxicity-targeted DDS provided superior therapeutic efficacy by increasing tumor tissue accumulation and enhancing cellular uptake, with low myelosuppression and systemic toxicity. We speculate that the combined strategy of targeting autophagic cell death may be a promising approach for the effective treatment of breast cancer by modulating autophagy and regulating apoptosis, so as to be extended to numerous tumor models with several other nanosystems.

Appendix A. Supporting information

Supporting data to this article can be found online at https://doi.org/10.1016/j.apsb.2019.03.006.

References

1. Miller KD, Siegel RL, Lin CC, Mariotto AB, Kramer JL, Rowland JH, et al. Cancer treatment and survivorship statistics, 2016. *CA Cancer J Clin* 2016;**66**:271−89.

2. Al-Lazikani B, Banerji U, Workman P. Combinatorial drug therapy for cancer in the post-genomic era. *Nat Biotechnol* 2012;**30**:679−92.

3. Yano S, Takeuchi S, Nakagawa T, Yamada T. Ligand-triggered resistance to molecular targeted drugs in lung cancer: roles of hepatocyte growth factor and epidermal growth factor receptor ligands. *Cancer Sci* 2012;**103**:1189−94.

4. Qin SY, Cheng YJ, Lei Q, Zhang AQ, Zhang XZ. Combinational strategy for high-performance cancer chemotherapy. *Biomaterials* 2018;**171**:178−97.

5. Liu Q, Qian Y, Li P, Zhang S, Wang Z, Liu J, et al. The combined therapeutic effects of ^{131}iodine-labeled multifunctional copper sulfide-loaded microspheres in treating breast cancer. *Acta Pharm Sin B* 2018;**8**:371−80.

6. Tian F, Dahmani FZ, Qiao J, Ni J, Xiong H, Liu T, et al. A targeted nanoplatform co-delivering chemotherapeutic and antiangiogenic drugs as a tool to reverse multidrug resistance in breast cancer. *Acta Biomater* 2018;**75**:398−412.

7. Yap TA, Omlin A, de Bono JS. Development of therapeutic combinations targeting major cancer signaling pathways. *J Clin Oncol* 2013;**31**:1592−605.

8. Duval AP, Jeanneret C, Santoro T, Dormond O. mTOR and tumor cachexia. *Int J Mol Sci* 2018;**19**:2225.

9. Toi M, Shao Z, Hurvitz S, Tseng LM, Zhang Q, Shen K, et al. Efficacy and safety of everolimus in combination with trastuzumab and paclitaxel in Asian patients with HER2$^+$ advanced breast cancer in BOLERO-1. *Breast Cancer Res* 2017;**19**:47.

10. Jovanović B, Mayer IA, Mayer EL, Abramson VG, Bardia A, Sanders ME, et al. A randomized phase II neoadjuvant study of cisplatin, paclitaxel with or without everolimus in patients with stage II/III triple-negative breast cancer (TNBC): responses and long-term outcome correlated with increased frequency of DNA damage response gene mutations, TNBC subtype, AR status, and Ki67. *Clin Cancer Res* 2017;**23**:4035−45.

11. Beck JT, Mantooth R. A case of disease improvement after treatment with everolimus plus exemestane in a patient with hormone receptor-positive metastatic breast cancer with bone metastases. *Case Rep Oncol* 2015;**8**:101−5.

12. André F, O'Regan R, Ozguroglu M, Toi M, Xu B, Jerusalem G, et al. Everolimus for women with trastuzumab-resistant, HER2-positive, advanced breast cancer (BOLERO-3): a randomised, double-blind, placebo-controlled phase 3 trial. *Lancet Oncol* 2014;**15**:580−91.

13. Huober J, Fasching PA, Hanusch C, Rezai M, Eidtmann H, Kittel K, et al. Neoadjuvant chemotherapy with paclitaxel and everolimus in breast cancer patients with non-responsive tumours to epirubicin/cyclophosphamide (EC) ± bevacizumab—results of the randomised GeparQuinto study (GBG 44). *Eur J Cancer* 2013;**49**:2284−93.

14. Gonzalez-Angulo AM, Akcakanat A, Liu S, Green MC, Murray JL, Chen H, et al. Open-label randomized clinical trial of standard neoadjuvant chemotherapy with paclitaxel followed by FEC *versus* the combination of paclitaxel and everolimus followed by FEC in women with triple receptor-negative breast cancer. *Ann Oncol* 2014;**25**:1122−7.

15. Mishra GP, Doddapaneni BS, Nguyen D, Alani AW. Antiangiogenic effect of docetaxel and everolimus as individual and dual-drug-loaded micellar nanocarriers. *Pharm Res* 2014;**31**:660−9.

16. Mishra GP, Nguyen D, Alani AW. Inhibitory effect of paclitaxel and rapamycin individual and dual drug-loaded polymeric micelles in the angiogenic cascade. *Mol Pharm* 2013;**10**:2071−8.

17. Wu MY, Fu J, Xu J, O'Malley BW, Wu RC. Steroid receptor coactivator 3 regulates autophagy in breast cancer cells through macrophage migration inhibitory factor. *Cell Res* 2012;**22**:1003−21.

18. Liu B, Bao JK, Yang JM, Cheng Y. Targeting autophagic pathways for cancer drug discovery. *Chin J Cancer* 2013;**32**:113−20.

19. Janku F, McConkey DJ, Hong DS, Kurzrock R. Autophagy as a target for anticancer therapy. *Nat Rev Clin Oncol* 2011;**8**:528−39.

20. Chen P, Cescon M, Bonaldo P. Autophagy-mediated regulation of macrophages and its applications for cancer. *Autophagy* 2013;**10**:192−200.

21. White E, Mehnert JM, Chan CS. Autophagy, metabolism, and cancer. *Clin Cancer Res* 2015;**21**:5037−46.

22. Mitra AK, Agrahari V, Mandal A, Cholkar K, Natarajan C, Shah S, et al. Novel delivery approaches for cancer therapeutics. *J Contr Release* 2015;**219**:248−68.

23. Dai W, Wang X, Song G, Liu T, He B, Zhang H, et al. Combination antitumor therapy with targeted dual-nanomedicines. *Adv Drug Deliv Rev* 2017;**115**:23−45.

24. Hare JI, Lammers T, Ashford MB, Puri S, Storm G, Barry ST. Challenges and strategies in anti-cancer nanomedicine development: an industry perspective. *Adv Drug Deliv Rev* 2017;**108**:25−38.

25. Muhamad N, Plengsuriyakarn T, Na-Bangchang K. Application of active targeting nanoparticle delivery system for chemotherapeutic drugs and traditional/herbal medicines in cancer therapy: a systematic review. *Int J Nanomed* 2018;**13**:3921−35.

26. Li Y, Song X, Yi X, Wang R, Lee SM, Wang X, et al. Zebrafish: a visual model to evaluate the biofate of transferrin receptor-targeted 7peptide-decorated coumarin 6 micelles. *ACS Appl Mater Interfaces* 2017;**9**:39048−58.

27. Song X, Li R, Deng H, Li Y, Cui Y, Zhang H, et al. Receptor mediated transcytosis in biological barrier: the influence of receptor character and their ligand density on the transmembrane pathway of active-targeting nanocarriers. *Biomaterials* 2018;**180**:78−90.

28. Ahlawat J, Henriquez G, Narayan M. Enhancing the delivery of chemotherapeutics: role of biodegradable polymeric nanoparticles. *Molecules* 2018;**23**:2157.

29. Vichai V, Kirtikara K. Sulforhodamine B colorimetric assay for cytotoxicity screening. *Nat Protoc* 2006;**1**:1112−6.

30. Chou TC. Theoretical basis, experimental design, and computerized simulation of synergism and antagonism in drug combination studies. *Pharmacol Rev* 2006;**58**:621−81.

31. Merkulova EA, Guiboileau A, Naya L, Masclaux-Daubresse C, Yoshimoto K. Assessment and optimization of autophagy monitoring methods in arabidopsis roots indicate direct fusion of autophagosomes with vacuoles. *Plant Cell Physiol* 2014;**55**:715−26.

32. Bao ZQ, Liao TT, Yang WR, Wang Y, Luo HY, Wang XZ. Heat stress-induced autophagy promotes lactate secretion in cultured immature boar Sertoli cells by inhibiting apoptosis and driving *SLC2A3, LDHA*, and *SLC16A1* expression. *Theriogenology* 2017;**87**:339−48.

33. Yu C, He B, Xiong MH, Zhang H, Yuan L, Ma L, et al. The effect of hydrophilic and hydrophobic structure of amphiphilic polymeric micelles on their transport in epithelial MDCK cells. *Biomaterials* 2013;**34**:6284−98.

34. Xu S, Olenyuk BZ, Okamoto CT, Hamm-Alvarez SF. Targeting receptor-mediated endocytotic pathways with nanoparticles: rationale and advances. *Adv Drug Deliv Rev* 2013;**65**:121−38.

35. Aissat N, Le Tourneau C, Ghoul A, Serova M, Bieche I, Lokiec F, et al. Antiproliferative effects of rapamycin as a single agent and in combination with carboplatin and paclitaxel in head and neck cancer cell lines. *Cancer Chemother Pharmacol* 2008;**62**:305−13.

36. Sendur MA, Zengin N, Aksoy S, Altundag K. Everolimus: a new hope for patients with breast cancer. *Curr Med Res Opin* 2013;**30**:75−87.

37. Wilks ST. Potential of overcoming resistance to HER2-targeted therapies through the PI3K//mTOR pathway. *Breast* 2015;**24**:548−55.

38. Costa RL, Han HS, Gradishar WJ. Targeting the PI3K/AKT/mTOR pathway in triple-negative breast cancer: a review. *Breast Cancer Res Treat* 2018;**169**:397−406.

39. Maes H, Agostinis P. Autophagy and mitophagy interplay in melanoma progression. *Mitochondrion* 2014;**19**:58−68.

40. Galluzzi L, Pietrocola F, Bravo-San Pedro J, Amaravadi RK, Baehrecke EH, Cecconi F, et al. Autophagy in malignant transformation and cancer progression. *EMBO J* 2015;**34**:856−80.

41. Lu HQ, Li GL, Liu LM, Feng LF, Wang X, Jin HC. Regulation and function of mitophagy in development and cancer. *Autophagy* 2013;**9**: 1720−36.

42. Detmer SA, Chan DC. Functions and dysfunctions of mitochondrial dynamics. *Nat Rev Mol Cell Biol* 2007;**8**:870−9.

43. Lemasters JJ, Nieminen A, Qian T, Trost LC, Elmore SP, Nishimura Y, et al. The mitochondrial permeability transition in cell death: a common mechanism in necrosis, apoptosis and autophagy. *Biochim Biophys Acta* 1998;**1366**:177−96.

44. Martinou JC, Green DR. Breaking the mitochondrial barrier. *Nat Rev Mol Cell Biol* 2001;**2**:63−7.

45. Eum KH, Lee M. Targeting the autophagy pathway using ectopic expression of Beclin 1 in combination with rapamycin in drug-resistant v-Ha-*ras*-transformed NIH 3T3 cells. *Mol Cells* 2011;**31**: 231−8.

46. Ding GB, Sun J, Wu G, Li B, Yang P, Li Z, et al. Robust anticancer efficacy of a biologically synthesized tumor acidity-responsive and autophagy-inducing functional beclin. *ACS Appl Mater Interfaces* 2018;**10**:5227−39.

47. Ren XQ, Chen YT, Peng HB, Fang XL, Zhang XL, Chen QY, et al. Blocking autophagic flux enhances iron oxide nanoparticle photothermal therapeutic efficiency in cancer treatment. *ACS Appl Mater Interfaces* 2018;**10**:27701−11.

48. Dai W, Yang F, Ma L, Fan Y, He B, He Q, et al. Combined mTOR inhibitor rapamycin and doxorubicin-loaded cyclic octapeptide modified liposomes for targeting integrin $\alpha 3$ in triple-negative breast cancer. *Biomaterials* 2014;**35**:5347−58.